Capturing essential physiological aspects of interacting cartilage and bone tissue with osteoarthritis pathophysiology: a human osteochondral unit-on-a-chip model

Tuerlings, M.; Boone, I.; Amirabadi, H.E.; Vis, M.; Suchiman, E.; Linden, E. van der; ... ; Meulenbelt, I.

ADVANCED MATERIALS TECHNOLOGIES
www.advmattechnol.de

Capturing Essential Physiological Aspects of Interacting Cartilage and Bone Tissue with Osteoarthritis Pathophysiology: A Human Osteochondral Unit-on-a-Chip Model

*Margo Tuerlings, Ilja Boone, Hossein Eslami Amirabadi, Michelle Vis, Eka Suchiman, Enrike van der Linden, Sandra Hofmann, Rob Nelissen, Jaap den Toonder, Yolande Ramos, and Ingrid Meulenbelt**

Given the multi-tissue aspects of osteoarthritis (OA) pathophysiology, translation of OA susceptibility genes towards underlying biological mechanism and eventually drug target discovery requires appropriate human in vitro OA models that incorporate both functional bone and cartilage tissue units. Therefore, a microfluidic chip is developed with an integrated fibrous polycaprolactone matrix in which neo-bone and cartilage are produced, that could serve as a tailored human in vitro disease model of the osteochondral unit of joints. The model enables to evaluate OA-related environmental perturbations to (individual) tissue units by controlling environmental cues, for example by adding biochemical agents. After establishing the co-culture in the system, a layer of cartilaginous matrix is deposited in the chondrogenic compartment, while a bone-like matrix is deposited between the fibers, indicated by both histology and gene expression levels of collagen type 2 and osteopontin, respectively. As proof-of-principle, the bone and cartilaginous tissue are exposed to active thyroid hormone, creating an OA disease model. This results in increased expression levels of hypertrophy markers integrin-binding sialoprotein and alkaline phosphatase in both cartilage and bone, as expected. Altogether, this model could contribute to enhanced translation from OA risk genes towards novel OA therapies.

1. Introduction

Osteoarthritis (OA) is an age-related degenerative joint disease, affecting more than 10% of the population over the age of 60 years.[1] The OA pathophysiological process is characterized by structural changes in both cartilage and the subchondral bone, including cartilage degeneration, subchondral bone thickening, and osteophyte formation. In absence of effective disease-modifying treatments, OA puts a high social and economic burden on society.[2] OA has a considerable genetic component and many studies have been performed highlighting the involvement of OA susceptibility.[3] The function of these genes merely involving maintenance processes in both bone and cartilage, confirms that aberrant molecular crosstalk between articular cartilage and subchondral bone plays an essential role in the initiation and progression of OA.[4] Furthermore, by applying molecular profiling of human OA articular cartilage, it has been consistently shown that activated

M. Tuerlings, I. Boone, H. E. D. Suchiman, Y. F. M. Ramos, I. Meulenbelt
Department of Biomedical Data Sciences
Section Molecular Epidemiology
Leiden University Medical Center
Leiden 2333 ZA, The Netherlands
E-mail: i.meulenbelt@lumc.nl

The ORCID identification number(s) for the author(s) of this article can be found under https://doi.org/10.1002/admt.202101310.

DOI: 10.1002/admt.202101310

H. Eslami Amirabadi, J. M. J. den Toonder
Department of Mechanical Engineering
Microsystems Section
and Institute for Complex MolecularSystems
Eindhoven University of Technology
Eindhoven 5600 MB, The Netherlands

M. A. M. Vis, S. Hofmann
Department. of Biomedical Engineering
Bioengineering Bone and Institute for Complex Molecular Systems
Eindhoven University of Technology
Eindhoven 5600 MB, The Netherlands

H. M. J. van der Linden, R. G. H. H. Nelissen
Department. Orthopaedics
Leiden University Medical Center
Leiden 2333 ZA, The Netherlands

articular chondrocytes with OA pathophysiology lose their healthy maturational arrested state and recapitulated an hypertrophic growth plate morphology with associated debilitating gene expressions.[5] To reliably mimic OA related chondrocyte hypertrophy, we recently showed that active thyroid hormone (Triiodothyronine, T3) could serve as a reliable trigger to induce OA related chondrocyte hypertrophy, marked by increased expression levels of *ALPL*, *RUNX2*, and *COL10A1*,[6] and eventually to the formation of bone.[7]

Given the multi-tissue function, translation of strong OA risk genes towards underlying biological mechanism, and eventually drug target discovery and testing require an appropriate human in vitro OA models that incorporate both functional bone and cartilage tissue units.[8] Such multi-tissue models require microfluidic tissue-on-chip systems that allow controllable automated flow in the different tissue compartment i.e. for culturing of chondrocytes and osteogenic cells separately in their preferred medium but in close contact with each other. Moreover, microfluidic chip technology allows OA-related environmental perturbations to (individual) tissue units by adding e.g., biochemical cues such as unbeneficial metabolites, cytokines, or factors inducing hypertrophy.[6c] Up until now, available microfluidic model systems mimicking osteochondral interaction are, however, hydrogel-based,[9] while ideally biological extracellular matrix (ECM) can be studied on top of cartilage and subchondral bone gene expression data.

To this end, we have developed a dual-tissue microfluidic device, that allows faithful engineering of functional interacting neo-cartilage and neo-bone tissues readily deposited by human primary osteogenic cells and human primary articular chondrocytes (hPACs) from patients that underwent joint replacement surgery due to OA (RAAK study).[10] Deposition of ECM by the primary cells was compared to our previously described 3D cell pellet culture model, which is epigenetically highly similar to autologous tissue.[11] As proof-of-principle, we evaluated whether we could mimic the dysfunctional adaptation processes of hypertrophic chondrocytes in our model, by exposing the system to T3. Henceforth, osteochondral unit-on-a-chip model could serve as a reliable biomimetic model to study tissue repair and regenerative capacity during OA.

2. Results

2.1. Microfluidic Chip Design

To allow engineering of functional interacting neo-cartilage and neo-bone tissues, a microfluidic chip was designed consisting of two channels that were separated by an electrospun polycaprolactone (PCL) matrix with a well-like structure on top of it. As shown in **Figure 1**A, the PCL matrix consists of a microfiber layer with thickness 190.1 ± 30.58 µm, fiber diameters of 8.60 ± 0.97 µm, and pore-sizes of 25.51 ± 12.37 µm (Figure 1B–C), and a nanofiber layer, with fiber diameters of 0.74 ± 0.55 µm and pore-sizes of 2.14 ± 1.14 µm (Figure 1 B–C). The microfiber layer served as a scaffold to seed and culture primary osteogenic cells, while the nanofiber layer will separate the primary osteogenic cells from the hPACs and prevent their migration to the other compartment. hPACs inherently prone to deposit high-quality cartilaginous tissue were seeded and cultured in high density in the well-like structure. Upon culturing primary osteogenic cells and hPACs for 28 and 21 days (Figure S1, Supporting Information), respectively, we harvested the constructs from the microfluidic chips and performed histology or we separated the two compartments for RT-qPCR. To determine the optimal time between media refreshment of the system to keep the chondro- and osteogenic media separate, we performed diffusion experiments using Dextran. Dextran was injected in the chondrogenic channel and after approximately 60 min fluorescence was measured in the osteogenic channel (Figure S2, Supporting Information).

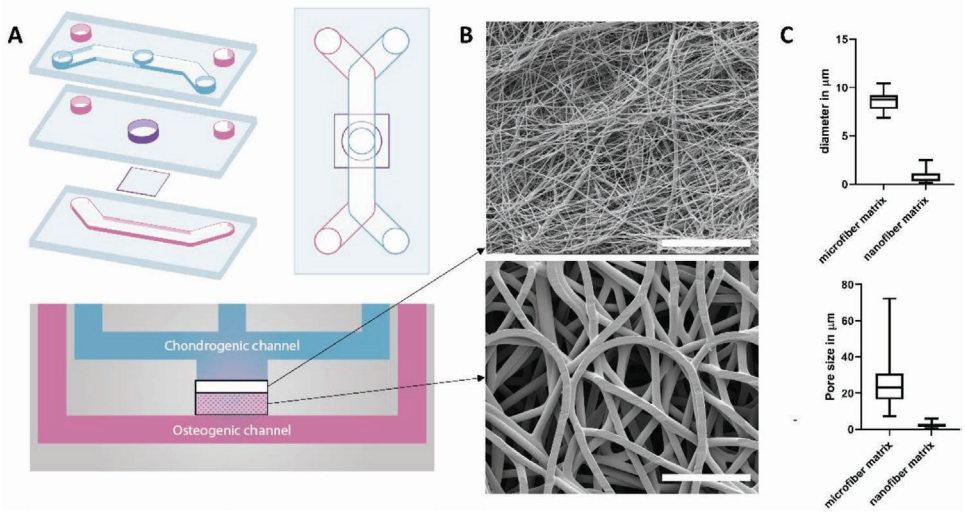

Figure 1. Osteochondral unit-on-a-chip model system. A) Schematic overview of the design of the microfluidic chip (blue: chondrogenic channel, pink: osteogenic channel, purple: co-culture compartment). B) Scanning electron microscopy pictures of the PCL electrospun matrix, with microfibers (bottom) and nanofibers (top). The white scalebar indicates 100 µm. C) Quantification of diameters and pore sizes of microfibers and nanofibers using the Quanta 600F ESEM software.

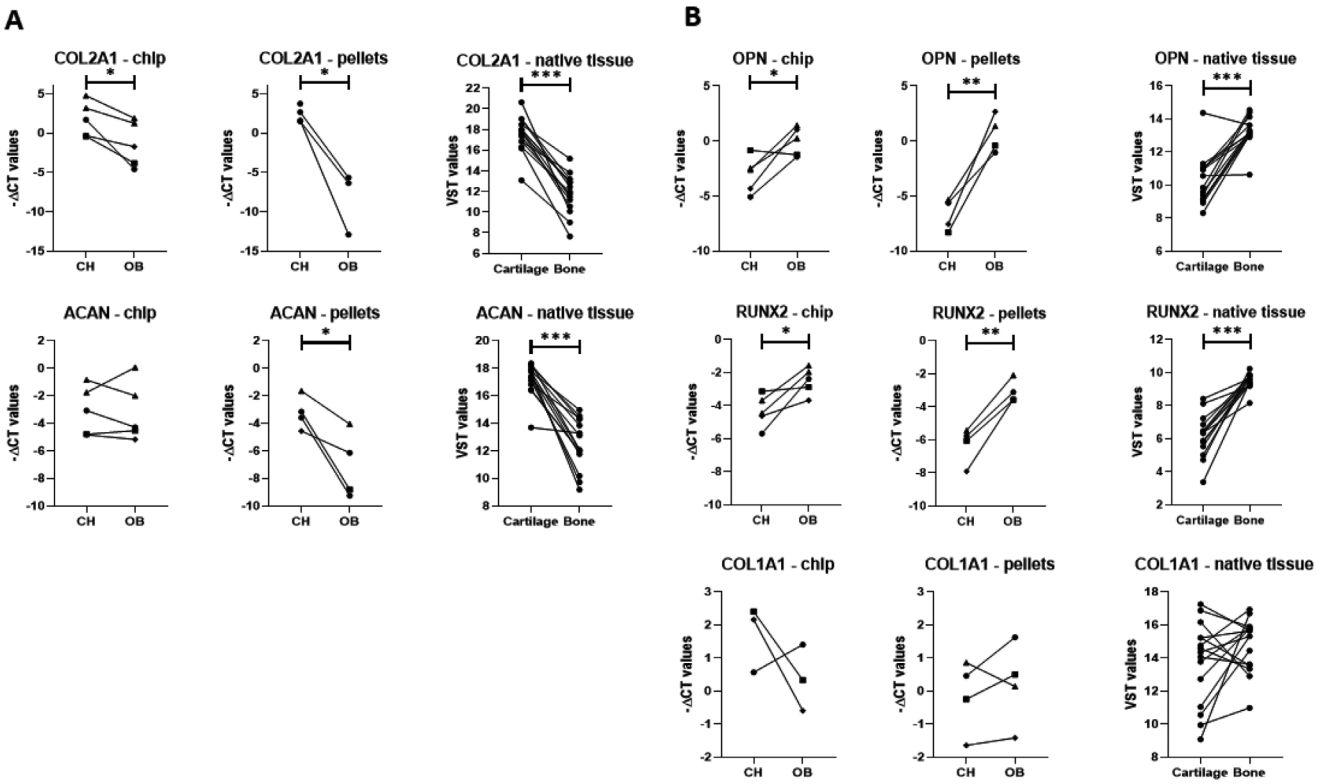

Figure 2. Gene expression levels of cartilage markers A) and bone markers B) measured in the osteochondral unit-on-a-chip model system (n = 3–4 donors, left panel), the 3D cell pellet cultures (n = 4 donors, middle panel), or the RNA-seq datasets (n = 15 donors, right panel). The chondrogenic compartment/chondrocyte cell pellet cultures are indicated with CH, while the osteogenic compartment and the osteogenic cell pellet cultures are indicated with OB. Paired sample t-test was used for statistical assessment, with * $p < 0.05$, ** $p < 0.005$, *** $p < 0.001$.

2.2. Gene Expression Analyses

Quality of chondrogenic and osteogenic matrix deposited in the chip was studied by means of RT-qPCR of cartilage markers *COL2A1* (encoding collagen type 2) and *ACAN* (encoding aggrecan) and bone markers *OPN* (encoding osteopontin), *RUNX2* (encoding RUNX Family Transcription Factor 2), and *COL1A1* (encoding collagen type 1), in comparison to our established 3D in vitro pellet culture model[11] of the same donors (n = 3–4 donors, Table S1A, Supporting Information). Moreover, we included gene expression data of our previously assessed RNA-sequencing datasets of autologous preserved bone and cartilage of patients that underwent a joint replacement surgery due to OA (n = 15 donors, Table S1B, Supporting Information).[5a,12] As shown in **Figure 2**A, we observed similar expression levels of *COL2A1* and *ACAN* between the chondrogenic compartment of the chip and the chondrocyte pellet cultures. Moreover, when comparing the chondrogenic to the osteogenic compartment, we observed higher expression of *COL2A1* (FC = 9.0, $p = 2.0 \times 10^{-2}$) in the chondrogenic compartment, which was in line with the 3D pellet cultures and RNA-seq data. As shown in Figure 2B, we observed similar expression levels of *RUNX2* and *OPN* between the osteogenic compartment of the chip and the osteogenic cell pellet cultures. Upon comparing the osteogenic compartment with the chondrogenic compartment, we observed higher expression of *RUNX2* (FC = 3.6, $p = 2.9 \times 10^{-2}$) and *OPN* (FC = 8.4, $p = 3.4 \times 10^{-2}$) (Figure 2B). Notably, *COL1A1* did not show similar expression levels between the chip and pellet cultures, as well as consistent differences between the osteogenic and chondrogenic compartment. These gene expression levels suggest that high-quality neo-bone and neo-cartilage matrix was deposited in our microfluidic model system after 28 days.

2.3. Neo-Bone and Cartilage Matrix Deposition

As shown in **Figure 3**A, a general Hematoxylin and Eosin (H&E) histological staining of the complete chip indicated the presence of two tissue types in the model system, a dense cartilage-like matrix with relatively high nuclei count on top of loose bone-like matrix. The matrix deposition in the osteochondral unit-on-a-chip model was assessed using several bone and cartilage stainings. Despite the fact that there was not a significant difference in *ACAN* expression levels between the chondrogenic and osteogenic compartment, we observed more intense Alcian Blue staining in the chondrogenic compartment, indicating higher glycosaminoglycan (GAG) content. The Alizarin Red staining showed calcium deposits at multiple locations of the osteogenic compartment of the chip, but not in the neo-cartilage (Figure 3C). This is in line with the more intense staining of bone marker OPN in the osteogenic compartment compared to the chondrogenic compartment (FC = 1.48, $p = 6.6 \times 10^{-2}$, Figure 3D). Both

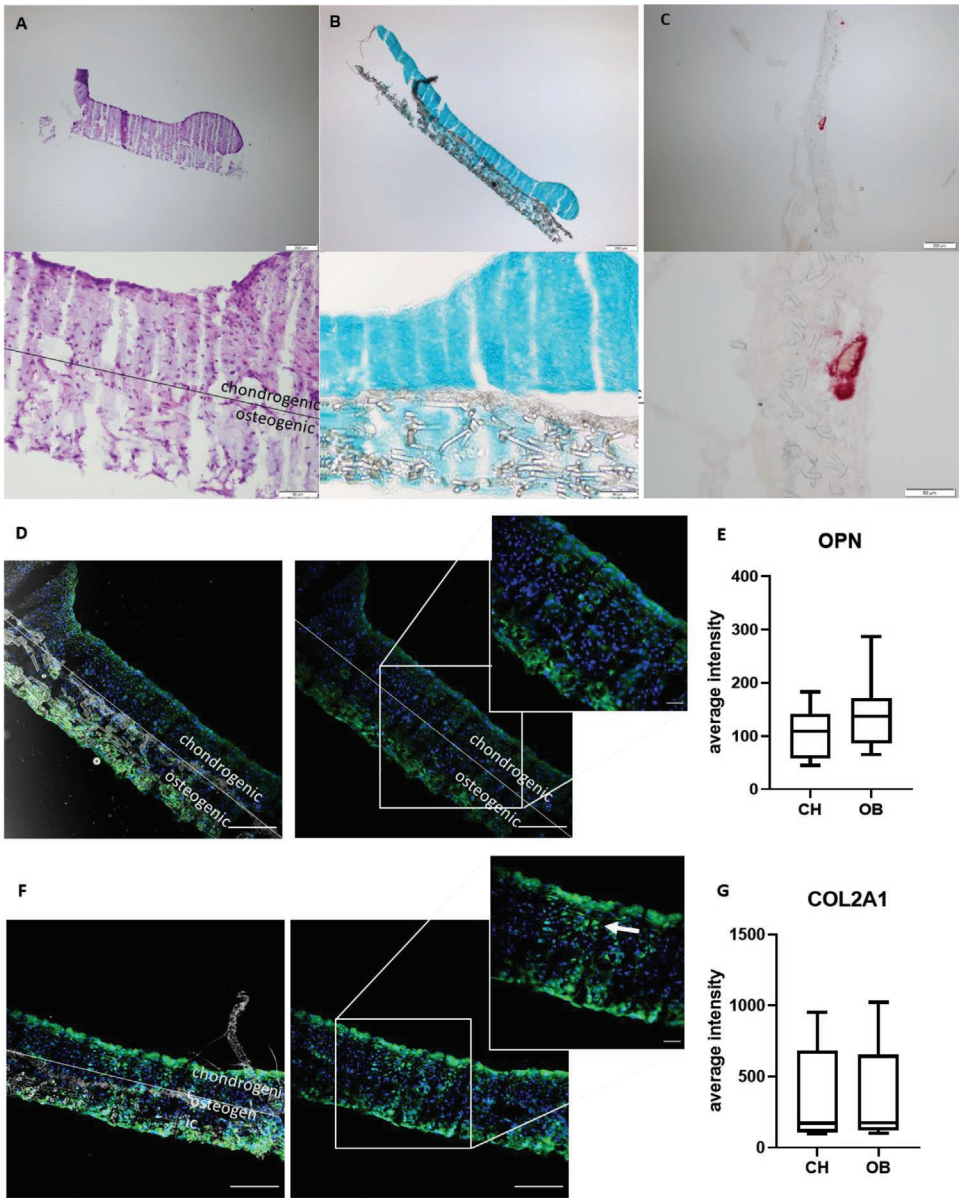

Figure 3. Representative images of (immuno-)histochemistry on cross sections of the osteochondral unit-on-a-chip system. A) Hematoxylin/ Eosin (H&E) staining. B) Alcian Blue staining. C) Alizarin red staining. D) OPN staining (in green) and DAPI staining (in blue). Overlap brightfield and fluorescence image (left) and fluorescence image (right). E) Quantification of OPN staining in average intensity ($n = 3$ donors). F) COL2A1 staining (in green) and DAPI staining (in blue). Overlap brightfield and fluorescence image (left) and fluorescence image (right). G) Quantification of COL2A1 staining in average intensity ($n = 3$ donors). Scalebar in smaller and larger magnification represents 200 µm and 50 µm, respectively. Two-sided paired sample *t*-test was used for statistical assessment of quantification, with * $p < 0.05$, ** $p < 0.005$, *** $p < 0.001$.

osteogenic staining suggest inhomogeneous distribution of cells throughout the matrix. Notably, most mineralization took place in the surface area of the bone matrix. As shown in Figure 3E, we observed COL2A1 staining in both compartments ($FC = 1.05$, $p = 1.26 \times 10^{-1}$), however, the staining appeared to be more structured (indicated by the arrow) in the chondrogenic compartment. Together, the gene expression findings and histology suggest the formation of two individual layers of cartilage- and bone like-matrix separated by the nanofiber PCL matrix.

2.4. Implementation of an OA Disease Model

To evaluate whether our biomimetic model can be used to study the effects of OA-related changes, we exposed both the chondrogenic and osteogenic compartments of our microfluidic chip to hypertrophy-inducing thyroid hormone T3, for 5 consecutive days ($n = 5$ donors, Table S1B, Supporting Information). Effects were determined by measuring expression levels of the chondrocyte hypertrophy markers *ALPL* (encoding alkaline phosphatase), *IBSP* (encoding Integrin

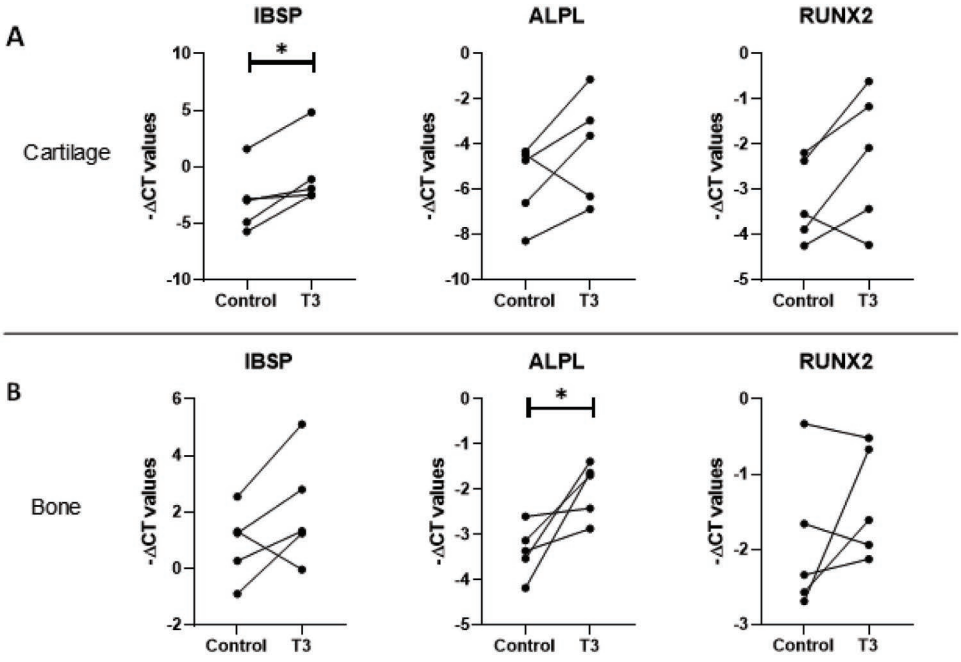

Figure 4. Gene expression levels of hypertrophy markers in the chondrogenic compartment A) and in the osteogenic compartment B) upon exposure to hypertrophy by adding T3 ($n = 5$ donors). Paired sample t-test was used for statistical assessment, with $^{*}p < 0.05$, $^{**}p < 0.005$, $^{***}p < 0.001$

Binding Sialoprotein), and *RUNX2*. As shown in **Figure 4**A, within the chondrogenic compartments we observed upregulation of hypertrophy markers *IBSP* ($FC = 5.04$, $p = 2.7 \times 10^{-2}$), *ALPL* ($FC = 2.83$), and *RUNX2* ($FC = 1.93$) upon comparing the hypertrophic and control chips, however *ALPL* and *RUNX2* did not reach statistical significance ($p = 0.172$ and $p = 0.104$, respectively). We did not observe consistent changes in the expression level of chondrogenic markers *ACAN* and *COL2A1* (Figure S3, Supporting Information). Within the osteogenic compartments we observed an upregulation of *ALPL* ($FC = 2.57$, $p = 4.1 \times 10^{-2}$) and *IBSP* ($FC = 2.29$) between the hypertrophic and control chips, however *IBSP* did not reach statistical significance ($p = 0.157$). Notably, *RUNX2* did not show a consistent direction of effect in the osteogenic compartment (Figure 4B). Similar variations in directions of effect were seen in the reference 3D pellet cultures (Figure S4, Supporting Information). These findings suggest that our microfluidic model system can serve as a hypertrophy-induced OA model to study concurrently cartilage and bone changes.

In addition, we collected medium from the system on the day starting the exposure (day 23) and the day of harvesting the osteochondral unit-on-a-chip system (day 28). To examine cartilage breakdown as a consequence of hypertrophy, we measured the sGAG release by performing a dimethylmethylene blue (DMMB) assay on the medium collected from the chondrogenic compartment ($n = 3$ donors). As shown in **Figure 5**, we observed increased sGAG release from day 23 to 28 in all three hypertrophic samples, while control samples showed variation (two samples decreased and one sample increased) in sGAG release. These results additionally show the possibility to perform multiple measurements on different time points for the same system during culture.

3. Discussion

Currently, there are no in vitro biomimetic OA models available that incorporate functional bone and cartilage tissue units, including biological matrix, in interaction. Here, we introduce a novel dual-tissue microfluidic model system in which interacting neo-cartilage and neo-bone are deposited. The current model allows for in-depth investigations of underlying mechanisms of OA risk genes beyond gene expression, towards a reliable biomimetic model of the osteochondral joint unit for tissue repair and regenerative capacity of primary osteogenic cells and hPACs upon OA related perturbations. Moreover, the model system can be used as

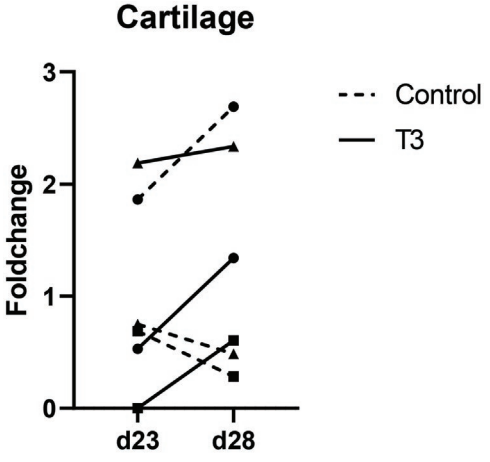

Figure 5. sGAG measurement in medium collected from the chondrogenic compartment on two different time points, before (day 23) and after (day 28) exposure to hypertrophy by adding T3 ($n = 3$ donors).

pre-clinical model for identification of druggable targets and for drug testing.

Upon culturing hPACs and osteogenic cells for 21 and 28 days, respectively, the osteogenic cells deposited osteogenic matrix in their compartment of the microfluidic chip, as indicated by the Alizarin Red and OPN staining (Figure 3C–E). The osteogenic nature of the matrix was confirmed by RT-qPCR, as bone markers *OPN* and *RUNX2* were highly expressed, while cartilage marker *COL2A1* was lowly expressed in the osteogenic compartment compared to the chondrogenic compartment (Figure 2). However, *ACAN* expression levels were relatively high in the osteogenic compartment. This, together with the lack of a calcified zone (Figure 3A) and the relatively low mineralization rate (Figure 3C), suggests the bone-like matrix in the system is not yet mature and therefore needs to be further optimized, for instance by extending the culture period or by homogenizing the distribution of osteogenic cells over the matrix. Upon culturing the hPACs for 21 days in our dual-tissue model system, we observed a thick layer of cartilaginous matrix deposited on top of the PCL matrix in the well-like structure as shown by the presence of GAGs (Figure 3B). Although COL2A1 staining was observed in both compartments (Figure 3F), the staining appeared to be more structured in the chondrogenic compartment. The difference in COL2A1 staining intensity between the chondrogenic and osteogenic compartment was minimal compared to the difference in OPN staining intensity between the two compartments, which confirmed the differences seen in gene expression levels (Figure 2). The H&E staining showed little difference in tissue morphology between chondro- and osteogenic compartments, which is partly due to the tears in the osteochondral construct as a result of sectioning. In contrast to the osteogenic compartment, we observed high gene expression levels of *COL2A1,* while low expression levels of *OPN* and *RUNX2* in the chondrogenic compartment, showing similar directions as both the well-established 3D pellet cultures[11] and the RNAseq of autologous cartilage and bone (Figure 2). The differences observed in gene expression levels between the osteogenic and chondrogenic compartments are smaller than the differences observed in the osteogenic and chondrogenic 3D cell pellet cultures, which might be due to the fact that within the chip we have a co-culture while the pellets are purely chondrocytes or osteogenic cells. Notably, *COL1A1* showed relatively high expression levels in both the osteogenic and chondrogenic compartments, while COL1 is known as an abundant protein in bone and is usually not present in healthy articular cartilage. Nonetheless, *COL1A1* is shown to be present in osteoarthritic articular cartilage,[13] which we also observe in our RNAseq data of the autologous macroscopically preserved cartilage from an end-stage OA joint. Therefore, *COL1A1* might not be a suitable bone marker when working with OA tissues.

Upon inducing hypertrophy by exposing the constructs to T3 for five consecutive days, we observed consistently increased expression levels of chondrocyte hypertrophy markers *IBSP*, *ALPL*, and *RUNX2* in the chondrogenic compartment. IBSP is a structural protein of bone matrix and ALP and RUNX2 are both osteoblastic markers. All three markers are known to be expressed by terminal hypertrophic chondrocytes.[14] The upregulation of these genes upon exposure to hypertrophy indicates that the gene expression pattern of the chondrogenic compartment changes towards an osteogenic phenotype, similar to OA pathophysiology and similar to the effects we observed in our previous study establishing a hypertrophic OA model.[6c] Despite the small sample size of the measurements on the collected medium, we show here the possibility to determine sGAGs at multiple timepoints during culture. The increase in sGAG release in the medium suggests that there was potentially more cartilage breakdown in hypertrophic constructs, which is in line with the OA phenotype. In the osteogenic compartment, *IBSP* and *ALPL* were also consistently upregulated in the hypertrophic compared to the control group, which may indicate increased bone formation upon inducing hypertrophy. This confirms the possibility of implementing disease-related perturbations to our chip to mimic pathophysiological processes. Therefore, our model system could serve as a platform for the identification of druggable targets and eventually drug testing. Together, this will contribute to cost-efficient preclinical research and reduce, refine, and replace animal experiments.

By introducing a novel dual-tissue microfluidic model system we established, for the first time, an osteochondral model in which interacting neo-cartilage and neo-osteogenic tissues are deposited by the primary cells. This is in contrast to currently available microfluidic model systems representing osteochondral construct based on cells encapsulated in specific hydrogels.[9] For example Lin et al.[9a] developed an osteochondral system consisting of two separate compartments to create chondrogenic and osteogenic microenvironments. Human bone marrow-derived stem cells were seeded in hydrogels inside this model system and UV was used to cure the hydrogel. Although this model attractively represents an osteochondral co-culture, the use of hydrogels has some disadvantages. The hydrogel requires UV or hydrogen peroxide exposure for its crosslinking, which may negatively influence primary cells by inducing cell senescence and adding potential uncertainty to the model.[15] In addition, hydrogels still fail to accurately mimic the 3D environment and a reoccurring problem is the formation of matrix islands within hydrogels, which occur because of the elastic nature of the material.[16] Moreover, the main disadvantage of the use of hydrogels instead of the formation of neo-tissue is that it limits the study output to only cell signaling and tissue repair upon perturbations is not visible.

Although we here showed that cartilaginous and osteogenic ECM were deposited in our microfluidic model system and that our model system can be used to study the effects of perturbations, further improvements to the model can still be made. In our previous studies,[6c,17] we showed that mechanical stress is an important trigger to OA onset and this type of perturbation cannot yet be captured by our model system. Hence, it would be added value to incorporate an actuation chamber to the model system, which can be used to apply mechanical stress to the construct and the cells within. In addition, to fully recapitulate an OA joint, implementation of other cell types such as synoviocytes, adipocytes, and immune cells would be preferable. Nevertheless, the most important hallmarks of OA are degeneration of articular cartilage and remodeling of subchondral bone. Moreover, genetic studies have indicated that aberrant molecular crosstalk between articular cartilage and subchondral bone plays a major role during OA pathophysiological process,

which can be studied using the here presented model.[4] In the current study, the model system was cultured under normoxic (20% oxygen) conditions while it is known that chondrocytes in vivo reside under hypoxic conditions (0-5% oxygen). Also, cells in the subchondral bone are exposed to lower oxygen levels (5%–10% oxygen) in vivo. Therefore, it might be beneficial to incorporate an oxygen gradient over the microfluidic chip or to culture the system under reduced oxygen levels. The primary cells used in the presented model system were isolated from end-stage OA joints. Primary cells are a finite cell source and the use of a more stable cell source, in the form of induced pluripotent stem cells (iPSCs), would be desirable. Using iPSCs in our model system would allow us to study, for example, high impact mutations in the interacting joint tissues bone, and cartilage, instead of focussing solely on one tissue. Finally, to ensure compatibility with high-throughput screens, of newly developed medication as part of pre-clinical studies and to minimize the amount of reagents required, the model system could even be further miniaturized and upscaled.

In conclusion, with this osteochondral unit-on-a-chip model system we indicate that it is possible to culture functional cartilage and bone tissue in vitro. This, together with the implementation of OA-related perturbation to this dual-tissue microfluidic chip, further advances the ongoing search for an appropriate multiple tissue interacting 3D-culture for multi-tissue diseases such as OA.[18] While this microfluidic chip is still further advancing, this model could contribute to enhanced translation from OA risk genes towards novel OA therapies.

4. Experimental Section

Sample Description: The current study includes $n = 24$ participants of the RAAK study, who underwent a joint replacement surgery as a consequence of OA. Material of four of these participants was used in the first set of experiments, in which we developed the osteochondral unit-on-a-chip system (Table S1A, Supporting Information). Material of five other participants was used in implementation of an OA-related disease model (Table S1C, Supporting Information). Material of the remaining participants was used for RNA sequencing (Table S1B, Supporting Information) donors was used. Informed consent was obtained from all participants of the RAAK study and ethical approval for the RAAK study was given by the medical ethics committee of the Leiden University Medical Center (P08.239/P19.013).

Electrospun Matrix: The matrix was fabricated by electrospinning polycaprolactone (PCL, Corbion Purac Biomaterials) as described previously.[19] Briefly, 18% PCL was dissolved in chloroform (anhydrous, amylene stabilized, Merck) for the microfibers, and 12% PCL was dissolved in chloroform: methanol (Merck). Electrospinning was done using the EC-CLI electrospinning apparatus (IME Technologies). The obtained matrices were characterized using scanning electron microscopy (SEM, Quanta 600F ESEM, Fei). To increase the conductivity of the surface, the matrices were sputter coated with gold prior to visualization. The quantification of the pore sizes was done by measuring the distance between fibers on at least 10 locations in at least six different images. The fiber diameter was measured in a similar way. For both quantifications, the Quanta 600F ESEM software was used.

Microfluidic Chip: The microfluidic chip was fabricated with a selective curing process as described previously.[19] Concisely, polydimethylsiloxane (PDMS, Dow Corning) without curing agent (PDMS-) was spincoated on a microscope glass slide. Then, the PCL matrix was applied on the spincoated PDMS-. PDMS with a curing agent (PDMS+, curing agent: PDMS- 1:10) was poured in a petri-dish, degassed, and partially cured at 65 °C. The partially cured PDMS was peeled off, cut into pieces with a surface area of ≈2 cm by 3.5 cm. Subsequently, a hole with a diameter of 4 mm was punched in the PDMS+, creating a well-like structure (middle layer with purple well-like structure, Figure 1A). Then, the well was aligned on top of the nanofiber matrix. PDMS+ was prepared, poured over the mould containing the structures of the microfluidic channels, degassed, and partially cured at 65 °C. The partially cured PDMS+ was peeled off, cut, and aligned with the well, after which it was left to completely cure overnight at room temperature. Subsequently, the cured structure was peeled off the glass slide and the holes for the in- and outlets were punched. Again PDMS+ was prepared, poured over the mould containing the channel structures, degassed, partially cured, peeled off, and cut, after which it was aligned with the matrix attached to the already cured structure. The chip was left at 40 °C to completely cure. The chip was flushed with isopropyl alcohol to remove the residuals of PDMS- from the matrix. Finally, female luers were attached to the in- and outlets.

Diffusion: Fluorescein isothiocyanate-dextran (Merck) was dissolved in a concentration of 2 mg ml^{-1} and added to the chondrogenic channel of an empty chip. Fluorescent images were obtained of the osteogenic channel every 5 min for 2 h at 37 °C using a fluorescent microscope (Leica, AF6000 LX). The average intensity was measured in these images using ImageJ.

Cell Culture: Primary osteogenic cells and hPACs were isolated from human joints as described previously.[6a,20] Isolation of primary osteogenic cells results in a mixture of bone cells, i.e., MSCs, osteoblasts, and osteocytes. Comparison of expression levels of osteogenic and chondrogenic markers of these cells with the expression levels in subchondral bone showed similar expression profiles [Tuerlings et al., under review]. Subsequently, the osteogenic cells and hPACs were expanded in 2D in osteogenic expansion medium (OBM) consisting of α-MEM + GlutaMAX (Thermofisher, 500 ml) supplemented with heat-inactivated FCS (10%, Biowest) and penicillin-streptomycin (Gibco, 0.2%, 10000 U ml^{-1}) and chondrogenic expansion medium (MSC medium) consisting of DMEM (Thermofisher, 500 ml) supplemented with FCS (10%, Biowest), penicillin-streptomycin (0.2%, 10000 U ml^{-1}) and FGF-2 (0.5 ng ml^{-1}, PeproTech), respectively.

Prior to seeding the cells in the microfluidic model system, the microfluidic chips were coated with fibronectin (Merck Chemicals), by flushing the system with fibronectin in PBS solution and incubate overnight. Osteogenic cells were seeded at a concentration of 6.0×10^6 cells ml^{-1} into the bottom compartment of the chip. After incubation to allow the cells to attach, the chip was connected to a syringe pump (Nexus 3000, Chemyx), programmed to withdraw medium from the system once every hour, with a flow of 50 µl min^{-1} in every channel. After 24 h, the OBM was replaced with osteogenic differentiation medium (ODM) consisting of α-MEM + GlutaMAX (Thermofisher, 500 ml) supplemented with heat-inactivated FCS (10%, Biowest), dexamethasone (0.1 µm; Sigma-Aldrich), L-ascorbate-2-phosphate (50 µg ml^{-1}, Sigma-Aldrich), and penicillin-streptomycin (0.2%, 10 000 U ml^{-1}).

After 6 days of culturing, hPACs were seeded in the upper compartment of the microfluidic chip via the middle inlet located directly above the matrix (Figure 1A) at a concentration of 1.5×10^7 cells ml^{-1}. After incubation to allow the hPACs to attach, the chip was reconnected to the syringe pump. After 24 h, both media reservoirs were refreshed: β-glycerophosphate (5mM; Sigma-Aldrich) was added to the ODM and MSC medium was replaced with chondrogenic differentiation medium consisting of DMEM (Thermofisher) supplemented with L-ascorbate-2-phosphate (50 µg ml^{-1}, Sigma-Aldrich), L-Proline (40 µg ml^{-1}, Sigma-Aldrich), Sodium Puryvate (100 µg ml^{-1}, Sigma-Aldrich), Dexamethasone (0.1 µm, Sigma-Aldrich), ITS+ (Corning), TGF-β1 (10 ng ml^{-1}, PeproTech), and antibiotics. In the T3-induced hypertrophy experiments, 500 ng ml^{-1} T3 was added to both media from day 23 onwards. After 28 days of culture, the chips were harvested for further processing. An overview of the experiment timeline is shown in Figure S1, Supporting Information. 3D pellet cultures were formed by adding 2.5×10^5 cells in their expansion medium to a 15 ml Falcon tube and subsequently exposing them to centrifugal forces. After 24 h, the expansion medium was

replaced by either osteogenic differentiation medium or chondrogenic differentiation medium. The medium was refreshed every 3–4 days.

Relative Gene Expression Levels: The two compartments were manually separated and were lysed using Trizol (Invitrogen) and stored at −80 °C until further processing. RNA was isolated from the samples using the RNeasy Mini Kit (Qiagen). cDNA synthesis was performed using the First Strand cDNA Synthesis Kit (Roche Applied Science). Subsequently, RT-qPCR was performed using SYBR Green without the ROX reference dye (Roche Applied Science) and the QuantStudio 6 Real-Time PCR system (Applied Biosystems). GAPDH and SDHA were used as housekeeping genes. The measured gene expression levels were corrected for the housekeeping genes GAPDH and SDHA, and the foldchanges were calculated using the $2^{-\Delta\Delta CT}$ method. All values were calculated relative to the control groups.

Histochemistry: For the different types of staining, the harvested materials were fixed with 4% formaldehyde, embedded in Tissue-Tek (Sakura), and sectioned at 25 µm thickness. After rehydration in PBS, Haematoxylin and Eosin staining was performed using the H&E stain Kit (Abcam). In addition, Alcian blue staining was performed using Alcian Blue 8-GX (Sigma) for 30 min and Alizarin red staining with Alizarin Red S (Sigma) for 1 min. All slides were mounted before brightfield imaging on Olympus BX53. Images were made with the Olympus DP26, using 4x and 20x objectives, and processed with Olympus cellSens Dimension 1.18 software. OPN and COL2 were visualized using immunohistochemistry. After rehydration, the tissue was blocked with 5% normal Goat serum (NGS, Sigma), incubated with primary rabbit anti-OPN antibody (HPA027541, Atlas antibodies) or with primary rabbit anti-COL2 antibody (ab34712, Abcam) followed by incubation of goat anti-rabbit Alexa Fluor 488 as the secondary antibody (ab150077, Abcam) and counterstained with DAPI prior to imaging on fluorescent microscope (Leica, AF6000 LX) with objectives HC PL FLUOTAR 10.0 × 0.30 DRY and HCX PL APO CS 20.0 × 0.75 DRY UV. Images were obtained with the Hamamatsu-C9100-02-COM4 camera and LASAF V2.7.4.10100 software and processed using ImageJ 1.53c.

DMMB Assay: sGAG concentration was measured in medium collected over 6 h from the chondrogenic compartment and measurements were done on two different time points, before (day 23) and after (day d28) exposure to hypertrophy by adding T3. Photometric 1.9 dimethylene blue (DMMB, Sigma Aldrich) dye was used to stain sGAGs, with Shark chondroitin sulfate (Sigma Aldrich) in culture medium as a reference. The collected medium from the chondrogenic compartment was diluted 30x, after which DMMB staining was added. Absorbance at 525 and 595 nm was measured using a microplate reader (Synergy HT, BioTek).

Statistical Analysis: For the RT-qPCR data, the minus delta CT values were used to perform the analysis. No outliers were visualized in the RT-qPCR data using boxplots. The RNA sequencing data was pre-processed as described previously[1] and variance stabilizing transformation was performed to normalize. The two-sided paired sample *t*-test was used to calculate significant differences in gene expression levels, considering p-value < 0.05 significant. Complete statistical output can be found in Table S2, Supporting Information. IBM SPSS Statistics, version 25 was used to perform all statistical analysis presented.

Supporting Information

Supporting Information is available from the Wiley Online Library or from the author.

Acknowledgements

The authors thank all the participants of the RAAK study. The LUMC had been and was supporting the RAAK study. The authors thank all the members of our group. The authors also thank Demiën Broekhuis, Robert van der Wal, Anika Rabelink-Hoogenstraaten, Peter van Schie, Shaho Hasan, Maartje Meijer, Daisy Latijnhouwers and Geert Spierenburg for collecting the RAAK material. The authors thank hDMT for rewarding this concept with the best hDMT Organ-on-Chip showcase award in 2018. The study was funded by the Dutch Scientific Research council NWO /ZonMW VICI scheme (nr 91816631/528) and VOILA – SMARTage (nr LSHM18093). Data was generated within the scope of the Medical Delta programs Regenerative Medicine 4D: Generating complex tissues with stem cells and printing technology and Improving Mobility with Technology. M. Tuerlings and I. Boone contributed equally to this work and Dr. Y.F.M. Ramos and Prof. Dr. I. Meulenbelt were shared it last.

Conflict of Interest

The authors declare no conflict of interest.

Data Availability Statement

The data that support the findings of this study are available on request from the corresponding author. The data are not publicly available due to privacy or ethical restrictions.

Keywords

cartilage, bone, joint on a chip, osteochondral construct, osteoarthritis, tissue engineering, tissue crosstalk

Received: October 7, 2021
Revised: March 2, 2022
Published online:

[1] a) D. Chen, J. Shen, W. Zhao, T. Wang, L. Han, J. L. Hamilton, H. J. Im, *Bone Res.* **2017**, *5*, 16044; b) Y. Krishnan, A. J. Grodzinsky, *Matrix Biol.* **2018**, *71–72*, 51; c) Y. Wu, E. L. Goh, D. Wang, S. Ma, *Open Access Rheumatol. Res. Rev.* **2018**, *10*, 135.

[2] A. Litwic, M. H. Edwards, E. M. Dennison, C. Cooper, *Br. Med. Bull.* **2013**, *105*, 185.

[3] a) C. G. Boer, K. Hatzikotoulas, L. Southam, L. Stefánsdóttir, Y. Zhang, R. Coutinho de Almeida, T. T. Wu, J. Zheng, A. Hartley, M. Teder-Laving, A. H. Skogholt, C. Terao, E. Zengini, G. Alexiadis, A. Barysenka, G. Bjornsdottir, M. E. Gabrielsen, A. Gilly, T. Ingvarsson, M. B. Johnsen, H. Jonsson, M. Kloppenburg, A. Luetge, S. H. Lund, R. Mägi, M. Mangino, R. Nelissen, M. Shivakumar, J. Steinberg, H. Takuwa, et al., *Cell* **2021**, *184*, 4784; b) U. Styrkarsdottir, S. H. Lund, G. Thorleifsson, F. Zink, O. A. Stefansson, J. K. Sigurdsson, K. Juliusson, K. Bjarnadottir, S. Sigurbjornsdottir, S. Jonsson, K. Norland, L. Stefansdottir, A. Sigurdsson, G. Sveinbjornsson, A. Oddsson, G. Bjornsdottir, R. L. Gudmundsson, G. H. Halldorsson, T. Rafnar, I. Jonsdottir, E. Steingrimsson, G. L. Norddahl, G. Masson, P. Sulem, H. Jonsson, T. Ingvarsson, D. F. Gudbjartsson, U. Thorsteinsdottir, K. Stefansson, *Nat. Genet.* **2018**, *50*, 1681; c) E. Zengini, K. Hatzikotoulas, I. Tachmazidou, J. Steinberg, F. P. Hartwig, L. Southam, S. Hackinger, C. G. Boer, U. Styrkarsdottir, A. Gilly, D. Suveges, B. Killian, T. Ingvarsson, H. Jonsson, G. C. Babis, A. McCaskie, A. G. Uitterlinden, J. B. J. van Meurs, U. Thorsteinsdottir, K. Stefansson, G. Davey Smith, J. M. Wilkinson, E. Zeggini, *Nat. Genet.* **2018**, *50*, 549.

[4] a) J. Pan, B. Wang, W. Li, X. Zhou, T. Scherr, Y. Yang, C. Price, L. Wang, *Bone* **2012**, *51*, 212; b) S. R. Goldring, M. B. Goldring,

Nat. Rev. Rheumatol. **2016**, *12*, 632; c) C. R. Fellows, C. Matta, A. Mobasheri, *EBioMedicine* **2016**, *11*, 2; d) R. J. Lories, F. P. Luyten, *Nat. Rev. Rheumatol.* **2011**, *7*, 43.

[5] a) R. Coutinho de Almeida, Y. F. M. Ramos, A. Mahfouz, W. den Hollander, N. Lakenberg, E. Houtman, M. van Hoolwerff, H. E. D. Suchiman, A. Rodriguez Ruiz, P. E. Slagboom, H. Mei, S. M. Kielbasa, R. Nelissen, M. Reinders, I. Meulenbelt, *Ann. Rheum. Dis.* **2019**, *78*, 270; b) W. den Hollander, Y. F. Ramos, N. Bomer, S. Elzinga, R. van der Breggen, N. Lakenberg, W. J. de Dijcker, H. E. Suchiman, B. J. Duijnisveld, J. J. Houwing-Duistermaat, P. E. Slagboom, S. D. Bos, R. G. Nelissen, I. Meulenbelt, *Arthritis Rheumatol.* **2015**, *67*, 2108.

[6] a) N. Bomer, W. den Hollander, Y. F. Ramos, S. D. Bos, R. van der Breggen, N. Lakenberg, B. A. Pepers, A. E. van Eeden, A. Darvishan, E. W. Tobi, B. J. Duijnisveld, E. B. van den Akker, B. T. Heijmans, W. M. van Roon-Mom, F. J. Verbeek, G. J. van Osch, R. G. Nelissen, P. E. Slagboom, I. Meulenbelt, *Ann. Rheum. Dis.* **2015**, *74*, 1571; b) M. B. Goldring, S. R. Goldring, *Ann. N. Y. Acad. Sci.* **2010**, *1192*, 230; c) E. Houtman, M. van Hoolwerff, N. Lakenberg, E. H. D. Suchiman, E. van der Linden-van der Zwaag, R. G. H. H. Nelissen, Y. F. M. Ramos, I. Meulenbelt, *Rheumatol. Ther.* **2021**, *8*, 499.

[7] a) R. Dreier, *Arthritis Res. Ther.* **2010**, *12*, 216; b) S. D. Bos, P. E. Slagboom, I. Meulenbelt, *Curr. Opin. Rheumatol.* **2008**, *20*, 553.

[8] D. Primorac, V. Molnar, E. Rod, Ž. Jeleč, F. Čukelj, V. Matišić, T. Vrdoljak, D. Hudetz, H. Hajsok, I. Borić, *Genes* **2020**, *11*, 854.

[9] a) H. Lin, T. P. Lozito, P. G. Alexander, R. Gottardi, R. S. Tuan, *Mol. Pharmaceutics* **2014**, *11*, 2203; b) Z. Lin, Z. Li, E. N. Li, X. Li, C. J. Del Duke, H. Shen, T. Hao, B. O'Donnell, B. A. Bunnell, S. B. Goodman, P. G. Alexander, R. S. Tuan, H. Lin, *Front. Bioeng. Biotechnol.* **2019**, *7*, 411; c) S. M. Goldman, G. A. Barabino, *BioRes. Open Access* **2016**, *5*, 109; d) C. C. Wang, K. C. Yang, K. H. Lin, H. C. Liu, F. H. Lin, *Biomaterials* **2011**, *32*, 7118.

[10] Y. F. Ramos, W. den Hollander, J. V. Bovee, N. Bomer, R. van der Breggen, N. Lakenberg, J. C. Keurentjes, J. J. Goeman, P. E. Slagboom, R. G. Nelissen, S. D. Bos, I. Meulenbelt, *PLoS One* **2014**, *9*, e103056.

[11] N. Bomer, W. den Hollander, H. Suchiman, E. Houtman, R. C. Slieker, B. T. Heijmans, P. E. Slagboom, R. G. Nelissen, Y. F. Ramos, I. Meulenbelt, *Osteoarthr. Cartil.* **2016**, *24*, 1423.

[12] M. Tuerlings, M. van Hoolwerff, E. Houtman, E. Suchiman, N. Lakenberg, H. Mei, E. van der Linden, R. Nelissen, Y. Ramos, R. Coutinho de Almeida, I. Meulenbelt, *Arthritis Rheumatol.* **2020**, *73*, 789.

[13] N. Miosge, M. Hartmann, C. Maelicke, R. Herken, *Histochem. Cell Biol.* **2004**, *122*, 229.

[14] a) T. Komori, *Cell Tissue Res.* **2010**, *339*, 189; b) J. C. Lui, S. Yue, A. Lee, B. Kikani, A. Temnycky, K. M. Barnes, J. Baron, *Bone* **2019**, *125*, 169; c) M. B. Mueller, M. Fischer, J. Zellner, A. Berner, T. Dienstknecht, L. Prantl, R. Kujat, M. Nerlich, R. S. Tuan, P. Angele, *Cells Tissues Organs* **2010**, *192*, 158; d) W. Liu, L. Zhang, K. Xuan, C. Hu, S. Liu, L. Liao, B. Li, F. Jin, S. Shi, Y. Jin, *Bone Res.* **2018**, *6*, 27.

[15] J. Duan, J. Duan, Z. Zhang, T. Tong, *Int. J. Biochem. Cell Biol.* **2005**, *37*, 1407.

[16] H.-p. Lee, L. Gu, D. J. Mooney, M. E. Levenston, O. Chaudhuri, *Nat. Mater.* **2017**, *16*, 1243.

[17] E. Houtman, M. Tuerlings, J. Riechelman, E. H. E. D. Suchiman, R. J. P. van der Wal, R. G. H. H. Nelissen, H. Mei, Y. F. M. Ramos, R. Coutinho de Almeida, I. Meulenbelt, *Arthritis Res. Ther.* **2021**, *23*, 215.

[18] S. Piluso, Y. Li, F. Abinzano, R. Levato, L. Moreira Teixeira, M. Karperien, J. Leijten, R. van Weeren, J. Malda, *Trends Biotechnol.* **2019**, *37*, 1063.

[19] H. Eslami Amirabadi, S. SahebAli, J. P. Frimat, R. Luttge, J. M. J. den Toonder, *Biomed. Microdevices* **2017**, *19*, 92.

[20] A. R. Stern, M. M. Stern, M. E. Van Dyke, K. Jähn, M. Prideaux, L. F. Bonewald, *BioTechniques* **2012**, *52*, 361.